Summary of thesis entitled

Catalytic materials based on Transition metals & Phosphomolybdate: Designing & Applications in some organic transformations

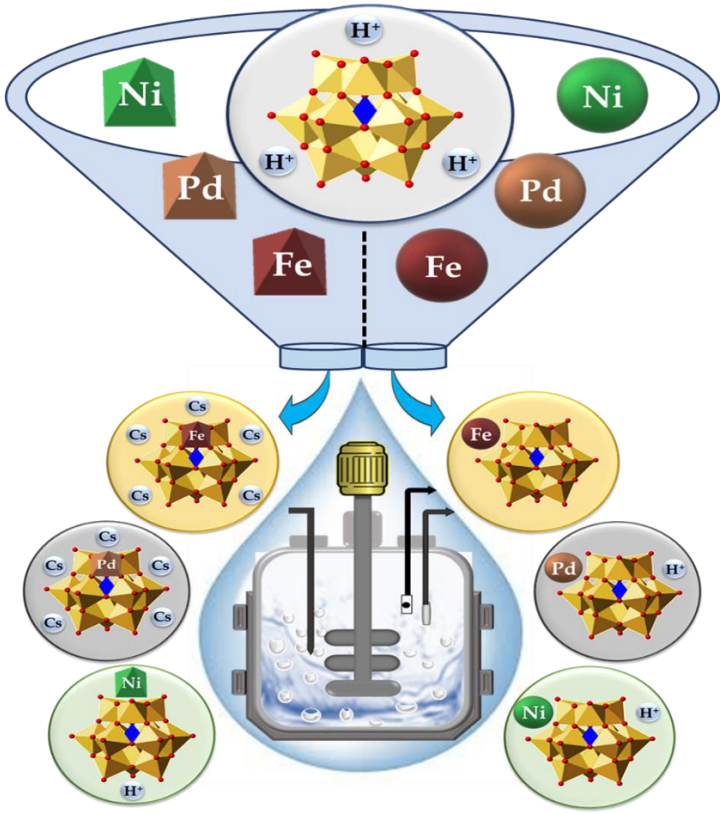

Submitted to
The Maharaja Sayajirao University of Baroda

For the Degree of

DOCTOR OF PHILOSOPHY
IN
CHEMISTRY

By

Mr. Jaykumar Patel

Department of Chemistry, Faculty of Science,
The Maharaja Sayajirao University of Baroda, Vadodara, 390 002.
Gujarat, INDIA

November, 2020

In 21st century, the key challenge of modern chemistry is to achieve 100% selectivity in the desired product in multipath reactions and to develop renewable energy-based processes [1]. To achieve this, catalysts are found to be one of the powerful tool because the designing of catalysts and catalytic systems provides key to obtain two goals, (i) environmental protection and (ii) economic benefits. The designing of advanced heterogeneous catalytic systems are feasible by the direct and controlled building of unique nanoscale and mesoscale structures, which leads to more efficient, benign, durable, and/or 'sustainable' catalytic systems [2].

In advancement to this, polyoxometalates (POMs) are excellent candidates for the same because they are the unique class of inorganic compounds having discrete metal–oxygen cluster composed of transition metals of group V and VI in high oxidation states [3-12]. They consist number of convergent properties such as robust oxoanionic nature, its negative charges, large relative sizes, stability, reducing and encapsulating agent as well structural diversity ranging from nano to micrometer scale [13]. Therefore, POMs have significant importance as they possess a wide variety of application in many areas such as catalysis [14-18], optics [19], electronic and electrochemical [20-22], magnetic [23, 24] and also in other fields like biology [25, 26], nano-materials [27-29] and surface sciences [30, 31].

With the development of POMs chemistry, various types of structures were discovered. Of all the different types of POMs, the Keggin type POMs are the most extensively studied because of its ease in synthesis, high thermal as well as chemical stability [3]. The ideal Keggin structure, $[XM_{12}O_{40}]^{3-}$ has T*d* symmetry and consists of a central XO_4 tetrahedron (X = central heteroatom) surrounded by twelve MO_6 octahedra (M = addenda atom). The twelve MO_6 octahedra form four groups of three edge-shared octahedra, the M_3O_{13} triplet, which have a common oxygen vertex connected to the central heteroatom. POMs have several advantages such as robust oxoanionic nature, Brønsted acidity, reversible redox

behaviour, high stability, reducing, encapsulating ability and most importantly, the structural mobility (by two ways; i. molecular levels and ii. available exchangeable protons).

Designing of POMs can be done at molecular level by four ways: (1) by formation of metal salt of POMs (2) by forming a defect (lacuna) in parent POMs structures (i.e. Lacunary Polyoxometalates, LPOMs), (3) by insertion of transition metal ions into the defected structures (i.e. Transition Metal Substituted Polyoxometalates, TMSPOMs) and (4) by supporting POMs on suitable support (Metal exchanged supported POMs).

1. Metal Salts of POMs

(a)

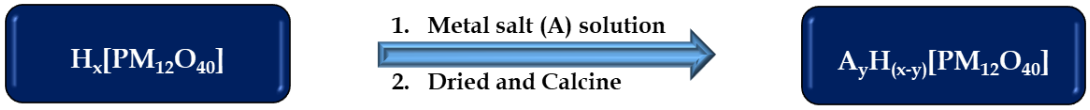

(b)

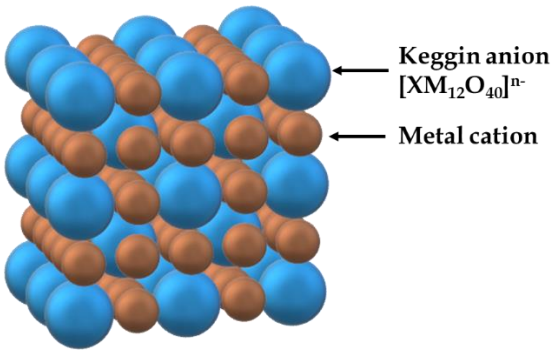

Scheme 1. (a) General synthetic route for metal salt of POMs and (b) BCC structure of Bulk metal salt of POMs

2. Lacunary POMs (LPOMs)

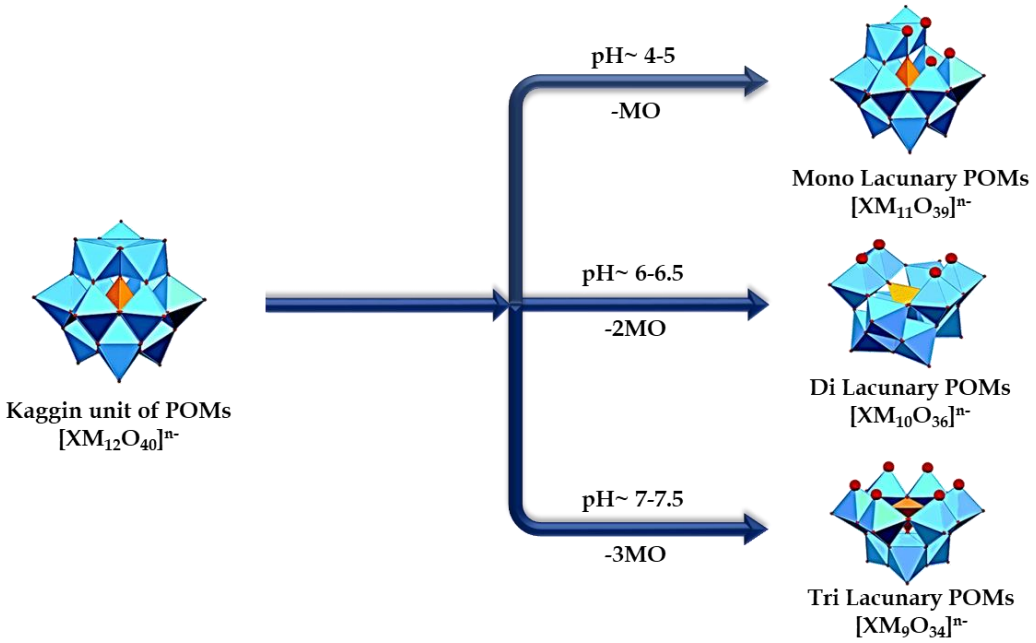

Scheme 2. pH dependent formation of LPOMs

3. Transition metal substituted POMs (TMSPOMs)

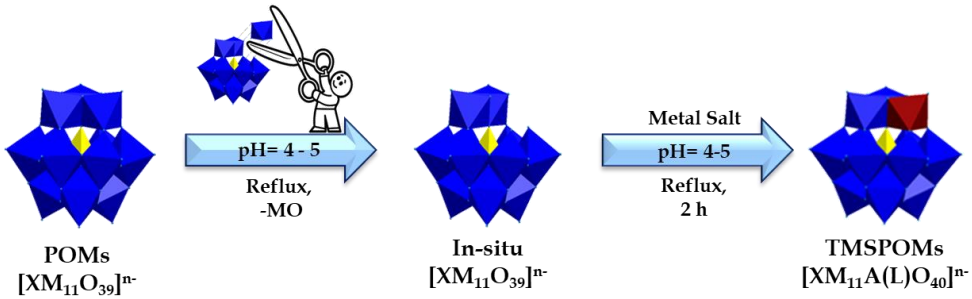

Scheme 3. General synthetic route for mono-transition metal substituted polyoxometalates

4. Supported POMs

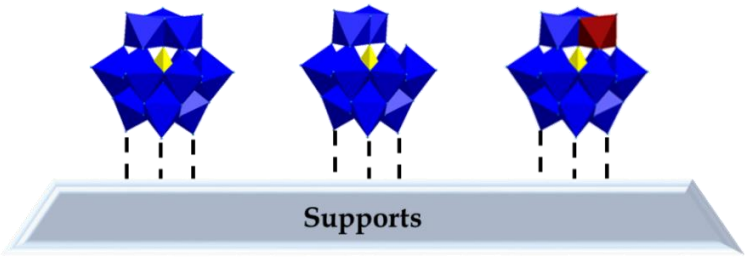

Scheme 4. Different types of supported POMs

Amongst various POMs, phosphomolybdic acid is known for their good redox property. A literature survey shows that phosphomolybdic acid based catalyst are less explored compared to phosphotungstic acid and silicotungstic acid based catalyst because of high decomposition and equilibrium rate as well as isolation of metal substituted phosphomolybdic acid from aqueous solution is quite difficult. So, it was thought of interest to synthesize, isolate and stabilize transition metal substituted or exchanged phosphomolybdic acid.

Considering these advantages and their ability to activate transition metal ions, a series of transition metal substituted or exchanged phosphomolybdic acid were synthesized. Fe, Pd and Ni were chosen as they are known to be redox active metal ions and they have wide range of catalysis, such as coupling, hydrogenation, oxidation, alkylation, acylation and many more.

Objectives of the Thesis

- To tune the structural and redox properties of lacunary phosphomolybdic acid by insertion of transition metal ions into the lacuna to form transition metal (Ni, Fe and Pd) substituted phosphomolybdic acid ($PMO_{11}Fe$, $PMo_{11}Ni$ and $PMo_{11}Pd$).
- To synthesize transition metal (Ni, Fe and Pd) exchanged phosphomolybdic acid supported on ZrO_2 as a support (Fe-PMo_{12}/ZrO_2, Ni-PMo_{12}/ZrO_2 and Pd-PMo_{12}/ZrO_2).
- To characterize synthesized materials by various techniques such as Elemental analysis, TG-DTA, FT-IR spectroscopy, Raman Spectroscopy, UV-Vis spectroscopy, ^{31}P NMR, ESR, XPS, Powder XRD, BET Surface area, SEM, TEM and HRTEM.
- To use the synthesized materials as catalyst for liquid phase hydrogenation of alkenes (styrene and cyclohexene) and levulinic acid, one-pot hydrogenation via C-C coupling.

- To study all the respective reaction parameters such as ratio of substrate to catalyst, temperature, pressure, time and solvent for maximum conversion as well as product selectivity.
- To study reaction mechanism.
- To propose best catalyst for each organic transformation.

This work is divided in to three parts based on transition metals

Part A: Designing of catalysts based on Iron & phosphomolybdic acid

Chapter 1: Cesium salt of iron substituted phosphomolybdate ($PMo_{11}Fe$): Synthesis, characterization and application for hydrogenation of styrene

Chapter 2: Iron exchanged phosphomolybdic acid supported on zirconia ($Fe\text{-}PMA/ZrO_2$): Synthesis, characterization and application for hydrogenation of cyclohexene

Part B: Designing of catalysts based on Nickel & phosphomolybdic acid

Chapter 1: Cesium salt of nickel substituted phosphomolybdate ($PMo_{11}Ni$): Synthesis, characterization and application for hydrogenation of levulinic acid

Chapter 2: Nickel exchanged phosphomolybdic acid supported on zirconia ($Ni\text{-}PMA/ZrO_2$): Synthesis, characterization and application for hydrogenation of levulinic acid

Part C: Designing of catalysts based on Palladium & phosphomolybdic acid

Chapter 1: Cesium salt of palladium substituted phosphomolybdate ($PMo_{11}Pd$): Synthesis, characterization and application for hydrogenation of levulinic acid

Chapter 2: Palladium exchanged phosphomolybdic acid supported on zirconia ($Pd\text{-}PMA/ZrO_2$): Synthesis, characterization and application for Suzuki–Miyaura cross coupling and One-pot Suzuki–Miyaura cross coupling/ nitro hydrogenation

Annexure: Nickel salt of phosphomolybdic acid (NiHPMA): Synthesis, characterization and application for oxidative esterification

Part A: Designing of catalysts based on Iron & Phosphomolybdic acid

Chapter 1: Cesium salt of iron substituted phosphomolybdate ($PMo_{11}Fe$): Synthesis, characterization and application for hydrogenation of styrene

Synthesis:

1.825 g of $H_3PM_{12}O_{40}$ was dissolved in minimum quantity of water and maintained at pH 4.3 followed by addition of saturated sodium bicarbonate

($NaHCO_3$) at 80 ^{0}C with stirring. To the resultant solution, saturated solution of 1 mmol of $Fe(NO_3)_3$ (0.404 g) was added. The final pH was maintained at 4.3 by adding $NaHCO_3$ solution and then refluxed at 80 ^{0}C for 1 h, filtered hot. Finally, to this saturated CsCl (5 mmol, 0.8418 gm) solution was added and the resulting yellow color precipitates were filtered, washed with water. It was further dried at room temperature and designated as $PMo_{11}Fe$.

Characterization:

Synthesized material was characterized by EDX, TGA FT-IR, Raman spectroscopy, ^{31}P NMR, ESR, XPS and powder XRD.

EDX mapping confirms the presence of Cs, P, Mo, Fe and O in synthesized materials. The observed EDX values of the elements (Cs:25.88%, P:1.27%, Mo:41.39%, Fe:2.08%, O:28.97%) were in good agreement with the that of calculated values (Cs:25.99%, P:1.21%, Mo:41.28%, Fe:2.18%, O:28.79%).

TGA shows 2.5% weight loss in the range of 30-100 ^{0}C, which is attributed to adsorbed water. Further, 1.3% weight loss is observed from 150 to 200 ^{0}C corresponding to loss of crystalline water. After that, no other significant weight loss is observed which indicate that the synthesized material is stable up to 500 ^{0}C. Based on elemental and thermal analysis, the formula of the complex is proposed as $Cs_5[PMo_{11}O_{39}Fe(H_2O)].5H_2O$

The FT-IR spectrum of $PMo_{11}Fe$ shows splitting in P-O band at 1070 and 1054 cm^{-1} due to decrease in symmetry of central atom PO_4 tetrahedron unit because of one MoO unit removal. The other bands at 964 cm^{-1}(M=O), 873 cm^{-1} (Mo-O_b-Mo) and 783 cm^{-1} (Mo-O_c-Mo), shows slight shifting because of the distortion introduced by one Mo replaced with Fe. Also, it shows one additional band at 516 cm^{-1} for Fe-O stretching frequency.

Raman spectra of $PMo_{11}Fe$ show peaks at 974, 928, 904, 603, and 223 cm^{-1} corresponding to v_s Mo=O, v_{as} Mo=O, v_{as} Mo-O_b-Mo, v_{as} Mo-O_c-Mo and v_{as} Mo-O_a stretching vibration respectively. Also, it shows peak at 367 cm^{-1}

corresponding to v_{as} O_a-P-O_a (central tetrahedral PO_4) stretching indicating that Keggin unit remains intact. $PMo_{11}Fe$ shows slight shifting due to insertion of Fe into lacuna by removing one MoO_t unit and obtained result is in good agreement with reported ones. ^{31}P MAS NMR of $PMo_{11}Fe$ was found to be silent due to insertion of Fe in lacuna by formation of paramagnetic spices (P-O-Fe^{3+}).

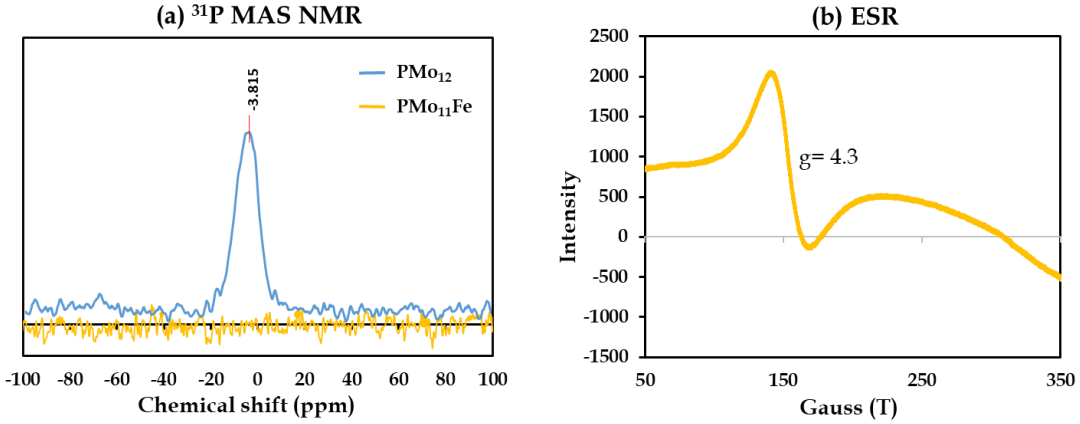

Figure 1. (a) ^{31}P MAS NMR and (b) ESR sepctra of $PMo_{11}Fe$ of fresh catalyst

The full range (5000–2500 G) X-band liquid nitrogen temperature ESR spectrum for $PMo_{11}Fe$ gives a single hyperfine spectrum with an isotropic signal, observed at g=4.3, which is assigned to Fe(III) with distorted octahedral geometry. It is integrated (incorporated) with phosphomolybdate in high-spin (3+ state).

The XPS of $PMo_{11}Fe$ show two intense doublet peaks at binding energy i) 233 and 235 eV, ii) 397 and 416 eV corresponding to $3d_{5/2}$, $3d_{3/2}$, $3p_{3/2}$ and $3p_{1/2}$ energy levels of Mo^{6+} respectively. Also, intense peak at 721 eV corresponds to 2p1/2 energy level of Fe^{3+}. Two additional high intense peaks at binding energy 532 eV and 724 eV are attributed to O1s and $Cs3d_{5/2}$, respectively.

The XRD patterns of PMo_{12} (figure 1d) show all characteristic peaks of 2θ in the range of 15^0 to 35^0. Similarly, XRD pattern of $PMo_{11}Fe$ (figure 1d) show all the characteristic peaks of Keggin unit, with slight shift due to Fe incorporation in PMo_{11} and also shows additional sharp peaks at 18.34, 23.88, and 30.28 attributed to the presence of Fe. Above study shows that Keggin unit remains preserved even after Fe in corporation.

The catalytic efficiency of $PMo_{11}Fe$ was evaluated for styrene hydrogenation. Effect of various reaction parameters such as solvent, substrate-catalyst ratio, reaction time, temperature, and H_2 pressure were studied to obtain maximum conversion.

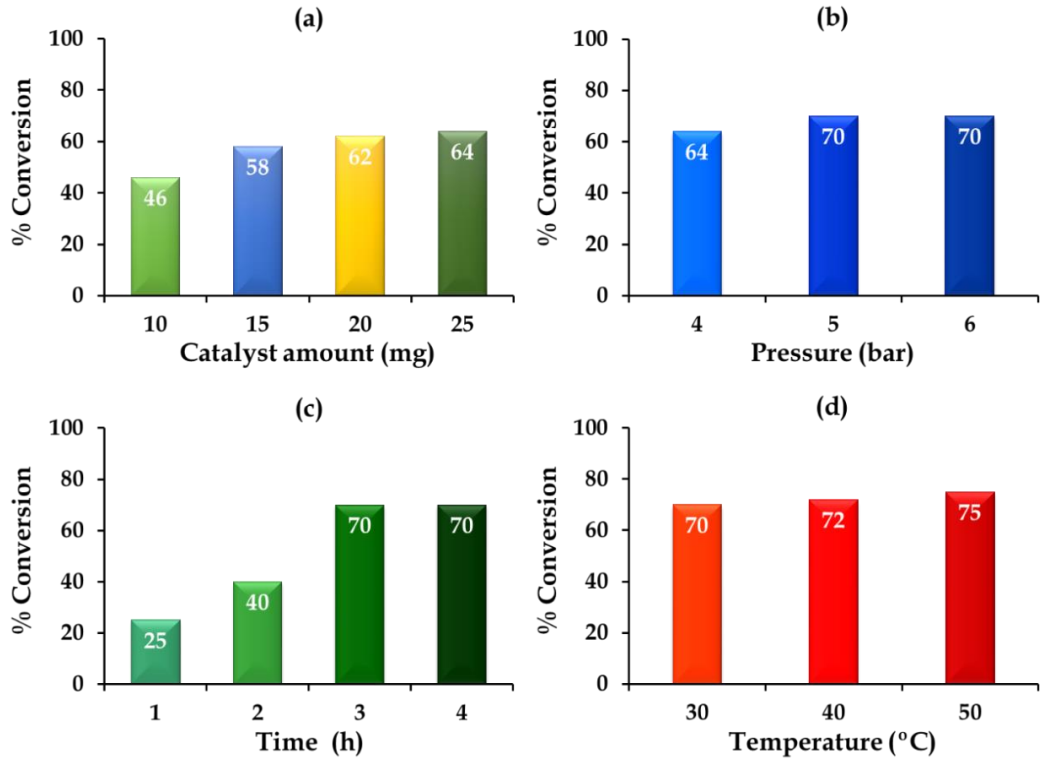

Figure 2. Optimization of reaction parameter for neat H_2O styrene hydrogenation. Reaction conditions: (a) Effect of catalyst amount- styrene (10 mmol), H_2 Pressure (5 bar), H_2O (50 mL), temperature (30 °C) and time (3 h); (b) Effect of pressure- cataalyst (25 mg), styrene (10 mmol), H_2O (50 mL), temperature (30 °C) and time (3 h); (c) Effect of temperature- cataalyst (25 mg), styrene (10 mmol), H_2O (50 mL), H_2 Pressure (5 bar), and time (3 h); (d) Effect of time- cataalyst (25 mg), styrene (10 mmol), H_2O (50 mL), H_2 Pressure (5 bar) and temperature (30 °C).

Initially, the reactions were carried out by varying the catalyst amount (Figure 2a) in the range of 25-5 mg with concentration of Pd(0) in the range of 0.1 mol% to 0.02 mol% respectively. It indicated that only 5 mg of catalyst (Fe: 0.02 mol%) is sufficient for the maximum % conversion. Effect of H_2 pressure was also carried out and obtained results represented that optimum 99% conversion was achieved at 5 bar pressure (Figure 2b). The influence of time on catalytic conversion indicates that 3 h is sufficient for maximum 99% conversion (Figure

2c). The effect of temperature was assesed between 60 to 90 °C and 99% conversion was obtained at 80 °C (Figure 2c).

The optimized conditions for maximum 70% conversion are: substrate /catalyst ratio (5081), catalyst (5 mg), Styrene (10 mmol), EtOH:H_2O (30:20 mL), H_2 pressure (5 bar), time (3 h) and temperature (30 ^{0}C) with TON (5081).

Styrene hydrogention in neat water

In an aqueous medium, the solvent study shows that in neat water 70% conversion was obtained. Therefore, effect of various parameters such as substrate to catalyst ratio, H_2 pressure, time and temperature have been studied using water as solvent to achieve maximum conversion.

The optimized condition for maximum 70% conversion are: catalyst amount (25 mg), active amount of Fe (0.1 mol%), styrene (10 mmol), substrate /catalyst ratio (1015), H_2 pressure (5 bar), time (3 h), temperature (30 °C), water (50 mL) and TON (710).

In order to investigate the role of individual components, control experiments were performed without H_2, without catalyst, using $Fe(NO_3)_3$ with active amount of Fe and with active amount of PMo_{11} under optimized reaction conditions. It was seen from the obtained result that H_2 pressure and catalyst both are essential for the reaction progress. Both $Fe(NO_3)_3$ and PMo_{11} gave low conversion in aqueous medium. This indicates that Fe of $PMo_{11}Fe$ is responsible for the reaction.

In order to check heterogeneity of $PMo_{11}Fe$, hot filtration test was carried out. The obtained result indicates that no leaching of Fe from $PMo_{11}Fe$ was observed during the reactions. This study indicates that the catalyst is truly heterogeneous in nature to be recycled and reused. To check sustainability of catalyst, the catalyst was recycled by simple centrifugation and reused for the next cycle. The obtained result show that there is no significant change in conversion up to two

cycles. This indicates that the catalyst is stable and can be reused up to several cycles.

The regenerated catalyst was characterized by EDX, FT-IR, ESR and XPS analysis for the confirmation of the catalyst structure retention.

The EDX values for regenerated $PMo_{11}Fe$ (Cs: 26.00%, P: 1.21%, Mo: 41.28%, Fe: 2.18%, O: 28.79%) is in good agreement with fresh one, indicating that there was no leaching of Fe during the reaction.

The FT-IR spectrum of fresh and regenerated catalysts show almost identical spectrum without any significant shift in characteristic band of regenerated $PMo_{11}Fe$ as compared to fresh $PMo_{11}Fe$, indicating that the structure of the catalyst remains unchanged even after regeneration. The ESR spectra of regenerated $PMo_{11}Fe$ gives a single hyperfine spectrum with an isotropic signal, observed at g=4.3, which is identical with fresh $PMo_{11}Fe$. The XPS of regenerated $PMo_{11}Fe$ show intense peaks at 234, 236, 397 and 416 eV which correspond to 3d, and 3p energy levels of Mo(VI) and also shows intense peak at 724 eV which corresponds to 2p energy level of Fe(III). The obtained spectrum is identical with fresh one, indicating sustainability of the catalyst.

To know the mechanistic pathway for styrene hydrogenation with the present catalyst ($PMo_{11}Fe$), control experiments as well as the reaction were carried out under N_2 pressure and D_2O as solvent. Control experiments confirmed that the Fe is the only active species and H_2 pressure is also essential for the progress of a reaction. Reaction was carried out under N_2 instead of H_2 and the obtained result (no conversion) shows that H_2 is essential for reaction progress when water acts as a solvent. Further, to confirm the role of water as solvent or proton transfer agent during the reaction, the reaction was carried out in D_2O instead of H_2O. The absence of the deuterated product in ^1H NMR indicates that the hydrogen was directly transferred from H_2 rather than water.

Further, to confirm any change in the oxidation state of Fe 3+ responsible for chemisorption, ESR spectra of the catalyst after quenching of reaction at 1 h, 1.5 h and 2 h were carried out. The ESR spectra of catalyst obtained after 1 h, 1.5 h and 2 h are similar with that of the fresh one, which confirms that no chemisorption takes place and the reaction proceeds through physisorption pathway.

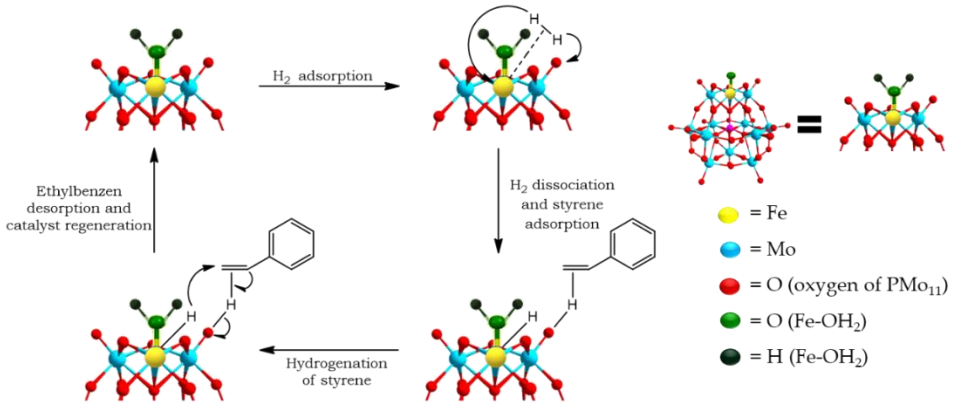

Scheme 5. Plausible mechanism of styrene hydrogenation.

Chapter 2: Iron exchanged phosphomolybdic acid supported on zirconia (Fe-PMo_{12}/ZrO_2): Synthesis, characterization and applications for hydrogenation of cyclohexene

To design the catalyst, the advantage of available counter protons of phosphomolybdic supported on zirconia was exploited. Iron exchange phosphomolybdic supported on zirconia were synthesized by following the same method reported by us. Iron exchanged supported phosphomolybdic acid was synthesized via exchanging the available protons of PMA. 1 g PMo_{12}/ZrO_2 was soaked with 25 mL 0.05 M $Fe(NO_3)_3$ aqueous solution with stirring for 24 hours. The solution was filtered, washed with distilled water to remove excess iron and dried in air at room temperature. The obtained yellow colored material was designated as Fe-PMo_{12}/ZrO_2.

The synthesized materials were characterized by characterized by EDX, TGA, FT-IR, ^{31}P NMR, ESR, XPS, powder XRD and HDDF-STEM.

The EDX mapping shows the presence of all elements. Found EDX values of Fe (0.54 wt%) and Mo (14.05 wt%) in Fe-PMo_{12}/ZrO_2 are in good agreement with theoretical calculated values of Fe (0.68 wt%) and Mo(14.14 wt%). TGA of Fe-PMo_{12}/ZrO_2 show 9.3% weight loss up to 100 ^{0}C due to the absorbed water. No weight loss observed up to 500 ^{0}C indicating stability up to 500 ^{0}C.

Fe-PMo_{12}/ZrO_2 (Figure 3a) shows all the characteristic bands of PMo_{12} at 1075 cm^{-1} (P-O_a), 948 cm^{-1}(M=O_t) and 887 cm^{-1} (Mo-O_b-Mo) as well as ZrO_2 at 1620 cm^{-1} (H-O-H), 1381 cm^{-1} (O-H-O) and a broad band at 700-400 cm^{-1} (Zr-O-H). However, minor shift in all bands may be attributed to the change in counter cation environment of PMo_{12}. Additional band of Fe-O stretching appears as a shoulder at 509 cm^{-1} due to its superimposition with that of broad band corresponding to Zr-O-H.

^{31}P MAS NMR of Fe-PMo_{12}/ZrO_2 (figure 4b) shows significant up filed shifting in peak from -5.13 ppm compared to PMo_{12}/ZrO_2 (-4.16 ppm). This is due to change in electronic environment of PMo_{12} as Fe gets exchanged with counter proton of PMo_{12}/ZrO_2. The temperature ESR spectrum of Fe-PMo_{12}/ZrO_2 (Figure 3b) shows a single isotropic hyperfine spectrum at g=4.3, which is allocated to Fe present in +3 states. The XPS analysis of Fe- PMo_{12}/ZrO_2 was recorded as shown in figure 3c. A binding energy peak at 724 eV corresponding to $Fe2p_{1/2}$ energy level, conforming the presence of Fe^{3+}. Similarly, spin-orbit binding energy level for Mo^{6+} was observed as two doublet i) at 233 and 235 eV corresponding to $3d_{5/2}$ and $3d_{3/2}$ energy level ii) at 397, and 416 eV corresponding to $3p_{3/2}$ and $3p_{1/2}$ energy level. Two additional intense peaks at binding energy 331 eV and 345 eV attributed to $Zr3p_{3/2}$ and $Zr3p_{1/2}$. Also, highly intense binding energy peak at 532 eV is attributed to O1s for oxygen present in PMA as well as ZrO_2.

The BET surface area of ZrO_2 is 170 m^2g^{-1} whereas the surface area of PMA/ZrO_2 is 204 m^2g^{-1}, which is significantly higher as compared to support ZrO_2 because of the strong interaction between PMo_{12} and support. However, the surface area

of Fe-PMo_{12}/ZrO_2 was found to be 208 m^2g^{-1}, this may be due to the exchange of Fe with available protons of PMo_{12}. The powder XRD pattern of Fe-PMo_{12}/ZrO_2 is similar to PMo_{12}/ZrO_2, indicating that Fe is highly dispersed on non-crystalline PMo_{12}/ZrO_2. HAADF-STEM images of Fe-PMo_{12}/ZrO_2 also confirm the homogeneous dispersion of Fe over the PMo_{12}/ZrO_2.

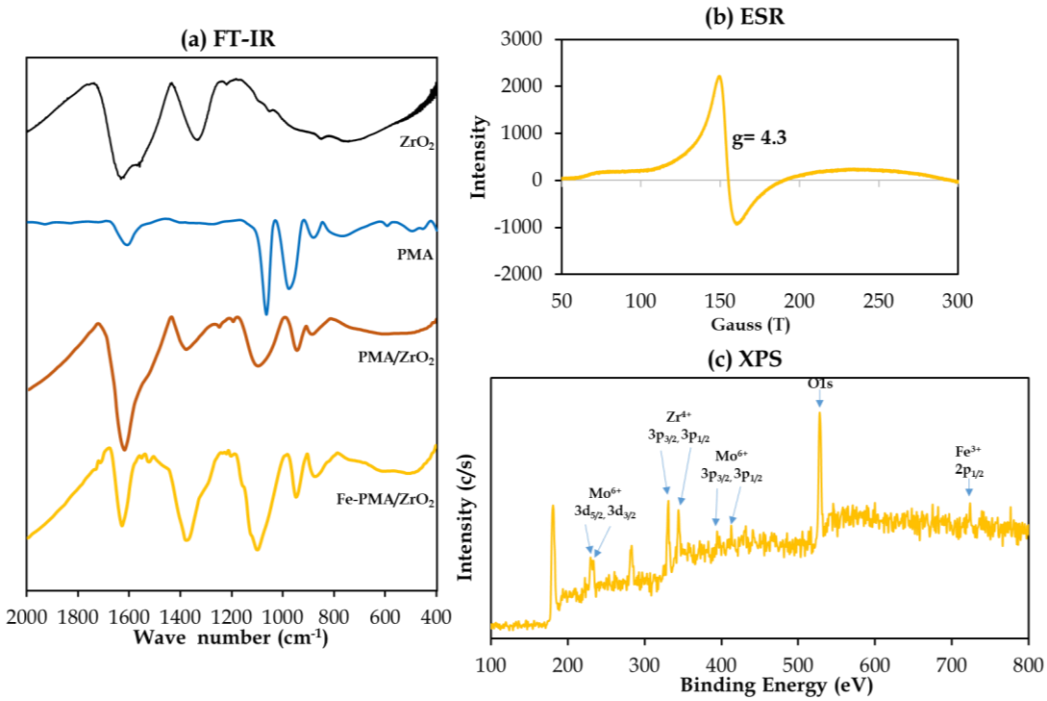

Figure 3. (a) FT-IR spectra, (b) ESR spectra and (c) XPS of Fe-PMo_{12}/ZrO_2

The catalytic activity of Fe-PMo_{12}/ZrO_2 was evaluated by performing hydrogenation of cyclohexene. In order to achieve maximum conversion, the effect of different reaction parameters (Figure 4) such as catalyst amount, temperature, pressure, time and solvent were studied.

The optimized conditions for maximum 90% conversion with 3742 TON are: catalyst amount (25 mg; Fe: 0.024 mol%), cyclohexene (9.87 mmol), H_2O (50 mL), H_2 pressure (10 bar), time (2 h) and temp. (50 °C), and Substrate/Catalyst ratio (4157/1).

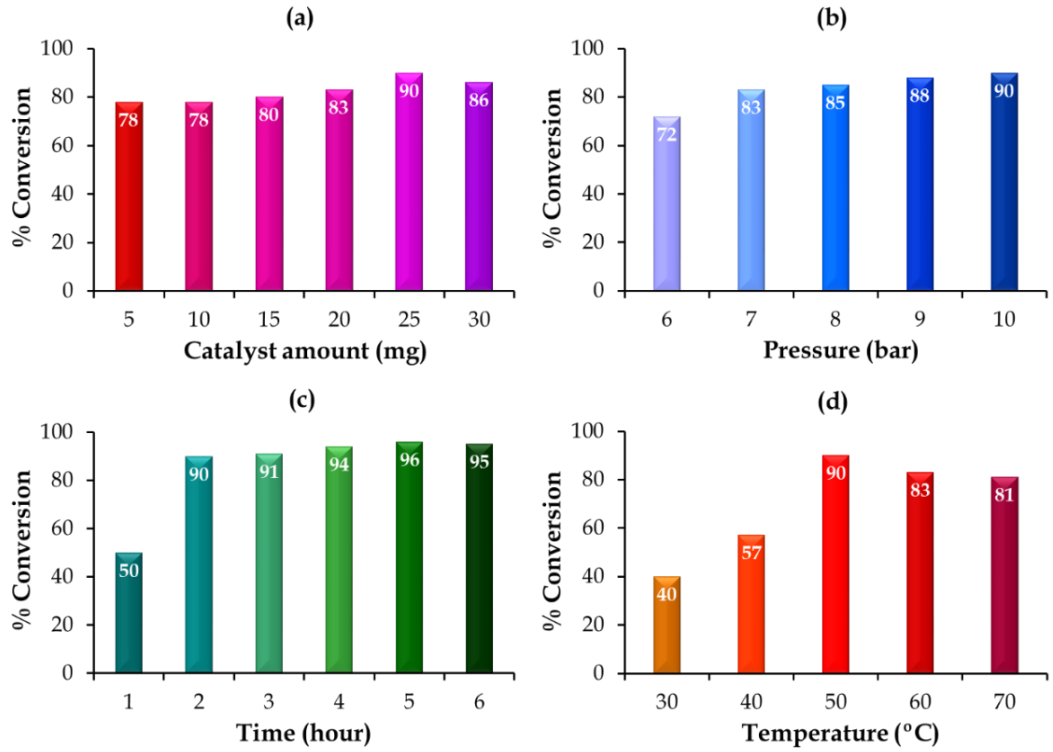

Figure 4. Optimization of reaction parameters for cyclohexene hydrogenation. Reaction conditions: (a) Effect of catalyst amount- Cyclohexene (9.87 mmol), H_2O (50 mL), H_2 pressure (10 bar), Time (2 h), temperature (50 °C); (b) Effect of H_2 pressure- Catalyst (25 mg), cyclohexene (9.87 mmol), H_2O (50 mL), time (2 h), temperature (80 °C); (c) Effect of time- Catalyst (25 mg), cyclohexene (9.87 mmol), H_2O (50 mL), H_2 pressure (10 bar), temperature (50 °C); (d) Effect of temperature: Catalyst (25 mg), cyclohexene (9.87 mmol), H_2O (50 mL), H_2 pressure (10 bar), time (2 h).

The control experiment indicates that Fe is the real active species responsible for the reaction. Whereas hot filtration and recyclability test confirms no leaching of Fe from Fe-PMo_{12}/ZrO_2. Therefore, it can be reused upto three cycles without significant loss in catalytic activity. In order to check the stability, the regenerated catalyst was characterized by EDX, FT-IR, ESR and XPS analysis which confirms the retention of catalyst structure even after recycled.

The comparison study shows that Fe-PMo_{12}/ZrO_2 is more active towards styrene and cyclohexene hydrogenation compered to PMo11Fe because of the position of catalytically active site present in designed catalyst as well as structural diversity of substrates.

Part B: Designing of catalysts based on Nickel & Phosphomolybdic acid

Chapter 1: Cesium salt of nickel substituted phosphomolybdate ($PMo_{11}Ni$): Synthesis, characterization and application for hydrogenation of styrene

Synthesis of cesium salt of nickel substituted phosphomolybdate ($PMo_{11}Ni$) was carried out by One-pot method. The synthesized catalyst was well characterized by basic physicochemical techniques such as EDX, TGA and FT-IR.

However, the synthesized catalyst was homogeneous in nature and during hydrogenation of styrene it got degraded. For this reason, we have not evaluated it for further catalytic studies.

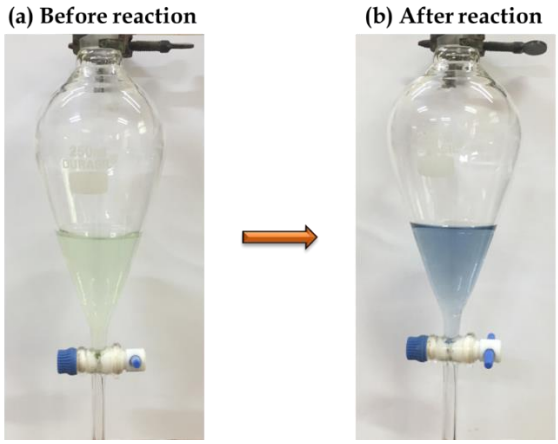

Figure 5. Color of homogeneous PMo11Ni (a)before reaction and (b) after reaction

Chapter 2: Nickel exchanged phosphomolybdic acid supported on zirconia (Fe-PMo_{12}/ZrO_2): Synthesis, characterization and applications for hydrogenation of styrene

Nickel was deposited on PMo_{12}/ZrO_2 via exchanging with the available protons of PMo_{12}. 1 g of PMo_{12}/ZrO_2 was soaked with 25 mL of 0.04 M aqueous solution of $Ni(CH_3CO_2)_2$ for 24 h with stirring. The solution was filtered, washed with distilled water in order to remove the excess of $Ni(CH_3CO_2)_2$ and dried in air at room temperature. The resulting green colored material was designated as Ni(II)-PMo_{12}/ZrO_2.

Synthesized material was characterized by elemental analysis, FT-IR, ^{31}P MAS NMR, XPS, BET surface area and Powder XRD.

The synthesized material was characterized by various physico-chemical techniques in which gravimetric as well as EDX showed the presence of Ni was 0.29 % wt. FT-IR, ^{31}P MAS NMR and powder XRD indicated the retention of the Keggin unit even after supporting PMo_{12} on ZrO_2 as well as exchanging Ni with available protons of PMo_{12}/ZrO_2. XPS confirmed the presence of Ni(II) and Mo(VI). BET surface area analysis of synthesized material shows small increase in surface area (208 $m^2\ g^{-1}$) as compared to PMo_{12}/ZrO_2, which further indicates that Ni is exchanged only with proton of PMo_{12}. N_2 sorption isotherms confirm the retention of the basic structure in the synthesized material.

The catalytic efficiency of the catalyst was evaluated towards levulinc acid hydrogenation reaction and various reaction parameters (effect of catalyst, formic acid, time, temperature and solvent) were optimized (Figure 10) to achieve maximum conversion.

Based on this study, the optimized conditions for 94% conversion are: Catalyst amount (50 mg), active amount of Ni ($2.47*10^{-3}$ mmol), LA (5 mmol), substrate /catalyst ratio (2024), FA (125 mmol), time (6 h) and temperature (200 °C) with TON (1902).

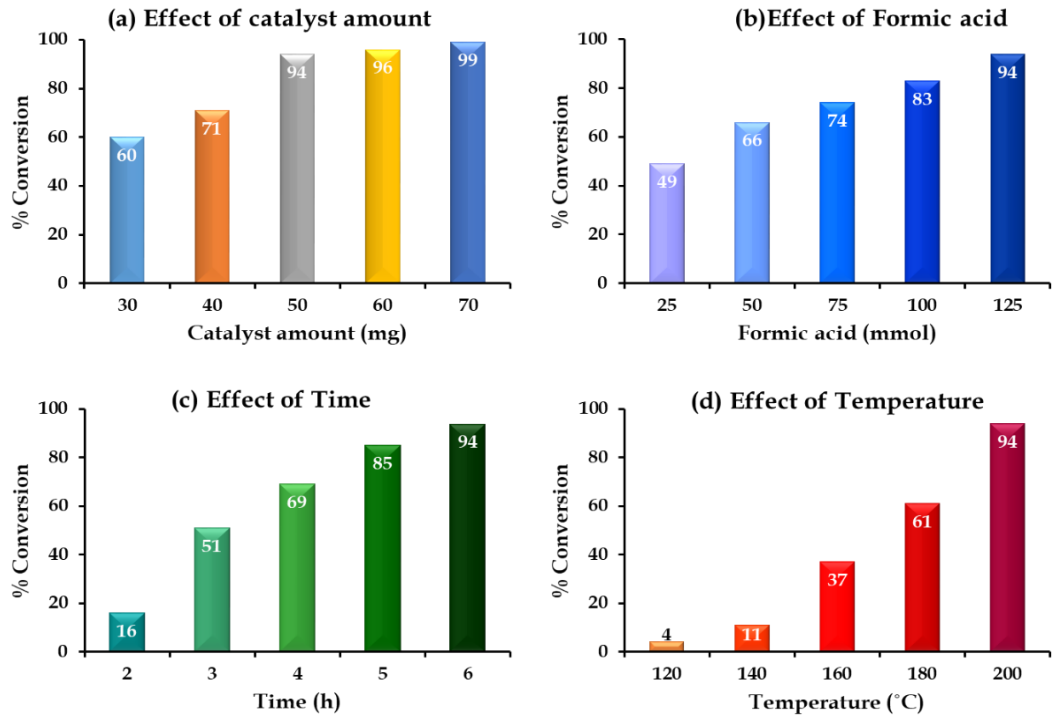

Figure 6. Optimization of reaction parameters for LA hydrogenation. Reaction conditions: (a) Effect of catalyst amount- LA (5 mmol), FA (125 mmol), time (6 h) and temperature (200 °C); (b) Effect of Formic acid- LA (5 mmol), catalyst (50 mg), time (6 h) and temperature (200 °C); (c) Effect of time. LA (5 mmol), FA (125 mmol), catalyst (50 mg) and temperature (200 °C); (d) Effect of temperature- LA (5 mmol), FA (125 mmol), catalyst (50 mg) and time (6 h).

Control experiments for all the three reactions indicate that Ni is the real active species responsible for the reaction. Whereas leaching and recycling test confirms the no emission of NiNPs as well as PMo_{12} from the support up to three catalytic runs. Heterogeneity test also confirms the true heterogeneous nature of the catalyst during the reactions.

Elemental analysis of regenerated catalyst shows the presence of all the expected elements and the found values for Ni (0.28 wt%) and Mo (14.13 wt%) are in good agreement with the theoretical values (Ni, 0.82 wt % and W, 14.16 wt%). FT-IR show the presence of all characteristic bands of fresh catalyst (Ni-PMo_{12}/ZrO_2), which confirms the retention of the Keggin structure. The XPS spectra indicates (Figure 7a) the presence of Ni (0) as well as Mo in VI oxidation states, which confirms the in-situ formation of NiNPs.

The BET surface area of R-Ni-PMo_{12}/ZrO_2 was found to be 219 m^2 g^{-1}, whereas drastic increase in surface area indicates the formation of Ni NPs. The N_2 sorption isotherm (Figure 7b) indicates the retention of basic structure of the material even after regeneration. XRD pattern of regenerated catalyst shows identical spectrum as fresh catalyst. The absence of any crystalline peaks confirms that there was no aggregates of NiNPS formed as well as retention of basic Keggin structure during the reaction. TEM and HRTEM images (Figure 7c) clearly show the presence of NiNPs with homogeneous dispersion over the amorphous surface of the PMo_{12}/ZrO_2. HAADF- STEM show high dispersion of Ni.

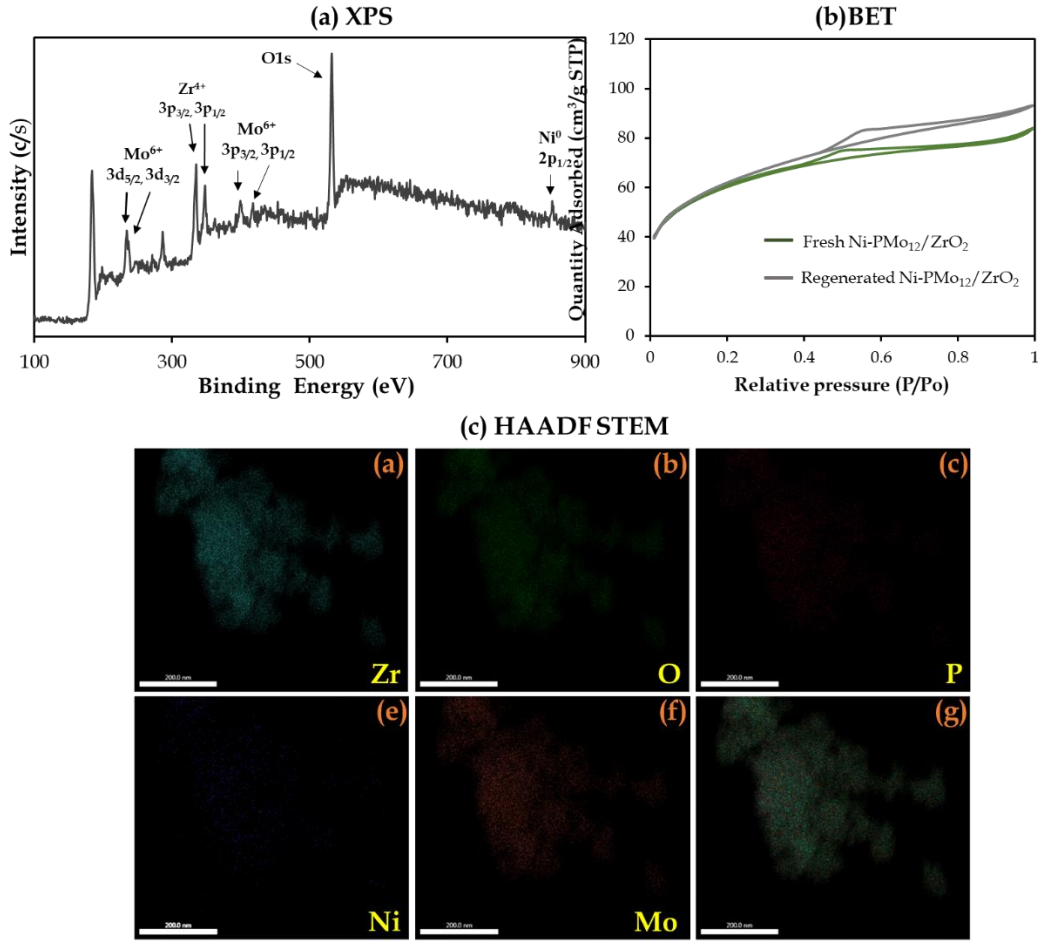

Figure 7. (a) XPS, (b) BET and (C) HAADF STEM of regenerated catalyst

To confirm formation of Ni(0), two sets of the reaction were carried out under optimized conditions. First, reaction was carried with Ni-PMo_{12}/ZrO_2 and FA

and the obtained catalyst was found to be black in color instead of light green, which confirms that initially Ni(II) gets reduced to Ni(0) via catalytic dehydrogenation of FA. To confirm this, further reaction was carried out without catalyst (reaction only with FA and LA) under optimized conditions and obtained result show 0% conversion of LA, because at high temperature, FA dehydrogenates to form H_2O and CO without the presence of any metal. The possible hydrogenation–dehydration mechanism was proposed based on the above study and is illustrated in scheme 6.

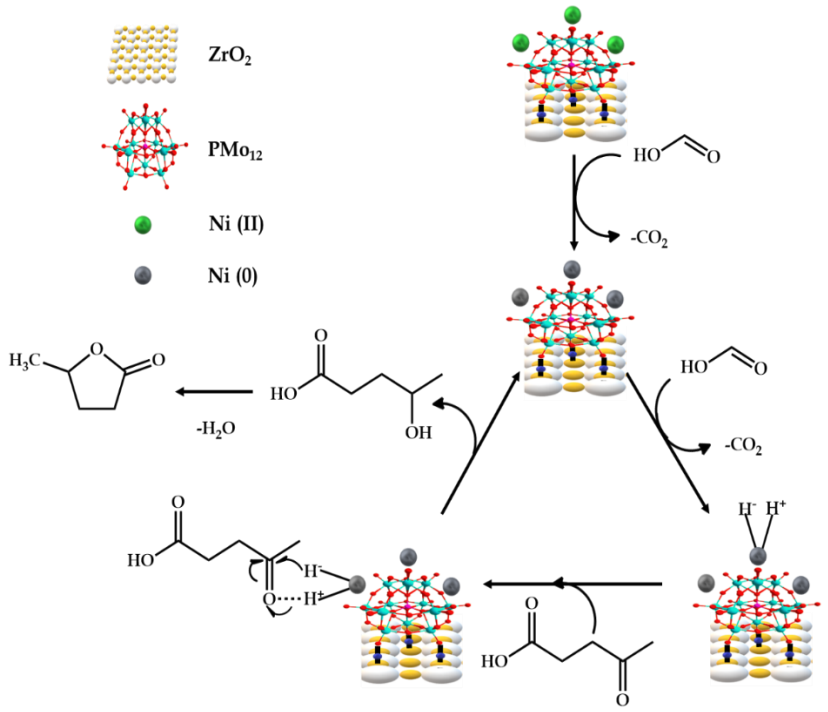

Scheme 6. Plausible LA hydrogenation reaction

Part C: Designing of catalysts based on Palladium & Phosphomolybdic acid

Chapter 1: Cesium salt of palladium substituted phosphomolybdate ($PMo_{11}Pd$): Synthesis, characterization and hydrogenation reaction

Cesium salt of palladium substituted phosphomolybdate was synthesized using one pot method as described in part A, chapter 1.

The synthesized material were characterized by elemental analysis (EDX), FT-IR, ^{31}P MAS NMR, XPS, powder XRD, TEM, HRTEM and HAADF-STEM.

Elemental analysis shows the presence of all the expected elements and the found values from EDX of the elements (Cs:25.43%, P:1.21%, Mo:40.28%, Pd:4.09%, O:28.97%) were in good agreement with that of calculated values (Cs:25.60%, P:1.19%, Mo:41.25%, Pd:44.11%, O:28.70%). FT-IR shows the presence of all the characteristic bands of PMo_{11} in the synthesized material $PMo_{11}Pd$, confirming the retention of the Keggin structure. ^{31}P MAS NMR shows significant down filed shifting in peak from 7.797 ppm which confirms that Pd is inserted in to the lacuna with retention of structure.

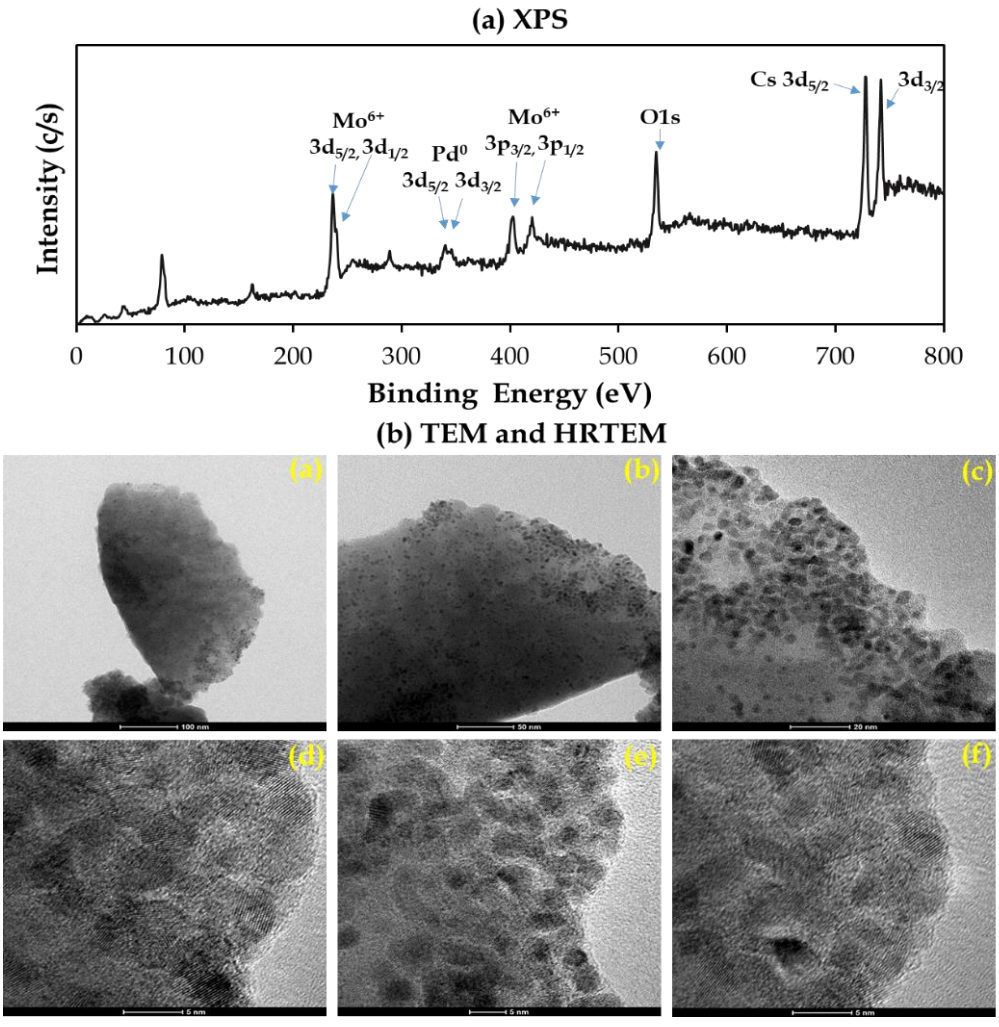

Figure 8. (a) XPS and (b) TEM and HR-TEM of $PMo_{11}Pd$

XRD pattern of the $PMo_{11}Pd$ showed all the characteristic peaks of Keggin unit, with slight shift due to Pd incorporation with PMo_{11}. The XPS spectra indicates (Figure 8a) the presence of PdNPs as well as Mo in VI oxidation states,

confirming no reduction of Mo(VI) during the synthesis of the materials. TEM and HRTEM images clearly show the presence of PdNPs, whereas HAADF – STEM images confirmed that high dispersion of Pd.

The catalytic efficiency of $PMo_{11}Pd$ was evaluated towards levulinic acid hydrogenation. In order to achieve maximum conversion, the effect of different reaction parameters such as catalyst amount, Formic acid, temperature, time and solvent was studied.

Based on this study optimized conditions for maximum 95% conversion are: Catalyst (5 mg, Pd: $1.879*10^{-3}$ mmol), substrate/catalyst ratio (2661), LA (5 mmol), FA (125 mmol), time (6 h), temperature (200 °C) and TON (2528).

The control experiments confirmed that Pd is the real active species which responsible for the reaction progress. Whereas hot filtration test confirms heterogeneous nature of the catalyst during the reactions and no emission of NiNPs as well as PMo_{12} from the support. The recyclability and reusability test shows that the synthesized catalyst is highly sustainable and it can be reused up to three catalytic runs without significant change in activity. The retention of retention of catalyst structure was confirmed by various physicochemical characterization techniques such as EDX, FT-IR, XPS and powder XRD. The hydrogenation–dehydration mechanism was proposed as described in chapter 2 (Part B). The synthesized catalyst was found to be superior as compared to reported Pd based catalyst.

Chapter 2: Palladium exchanged phosphomolybdic acid supported on zirconia ($Pd\text{-}PMo_{12}/ZrO_2$): Synthesis, characterization and One-pot Suzuki–Miyaura cross coupling/ nitro hydrogenation

Palladium was deposited on PMo_{12}/ZrO_2 via exchanging the available protons of PMA by ion exchange method as described part A chapter 1. The resulting (brown colored) material was designated as Pd(II)- PMo_{12}/ZrO_2. Finally, the synthesized material was charged in a Parr reactor under 1 bar H_2 pressure, at

40 °C for 30 min to reduce Pd(II) to Pd(0). The obtained (black colored) material was designated as Pd- PMo_{12}/ZrO_2.

Synthesized material was characterized by elemental analysis, FT-IR, ^{31}P MAS NMR, XPS, BET surface area, powder XRD, TEM, HRTEM and HAADF-STEM.

The gravimetric analysis shows 0.43 %wt of Pd in Pd(II)-PMo_{12}/ZrO_2 as well as elemental analysis by EDX also shows 0.45 %wt of palladium in Pd-PMo_{12}/ZrO_2. The TGA of the Pd-PMo_{12}/ZrO_2 shows the 9.3 % weight loss up to 200 °C due to the loss of adsorbed water molecules. No weight loss was observed up to 500 °C indicating the stability of the catalyst up to 470 °C.

The FT-IR spectrum (figure 6a) of Pd- PMo_{12}/ZrO_2 shows the characteristic bands at 1078, 956, 878 and 790 cm^{-1} corresponding to stretching vibration of P=O, Mo=O and Mo-O-Mo with significant shift, may be due to the change in counter cation environment of PMA due to insertion of Pd. Here, additional band corresponding to Pd-O is not observed, this may be due to the merging of band with Zr-O.

^{31}P MAS NMR of Pd- PMo_{12}/ZrO_2 (figure 6b) shows significant up filed shifting in peak from -4.1 to -5.61 ppm as compared to PMo_{12}/ZrO_2. This is due to change in electronic environment of PMA as Pd gets exchanged with counter proton of PMo_{12}/ZrO_2.X-ray photoelectron spectroscopy (XPS) of Pd- PMo_{12}/ZrO_2 was recorded (figure 6c). It displayed two low intense peaks at 334.78 eV and 340.16 eV, corresponding to two distinct spin-orbits $3d_{5/2}$ and $3d_{3/2}$ respectively of the metallic palladium (Pd^0), which confirms the formation of PdNPs. Two different intense peaks at 233 eV and 235 eV corresponding to spin-orbits $3d_{5/2}$ and $3d_{3/2}$ of Mo^{6+} respectively, confirms that Mo(VI) is not reduced during reduction of Pd(II) to Pd(0).

The BET surface area of Pd- PMo_{12}/ZrO_2 (228 $m^2\ g^{-1}$) show that there is a drastic increase in the value of surface area as compared to that of Pd(II)- PMo_{12}/ZrO_2 (208 $m^2\ g^{-1}$), confirming the reduction of Pd(II) to Pd(0) and is in good agreement

with the known fact that nanoparticles have higher surface area than the parent one. In XRD patterns of Pd-PMo_{12}/ZrO_2, absence of any crystalline peak corresponds to Pd(0), which is due to the low concentration of Pd(0) on the surface of the catalyst as well as high dispersion of PdNPs on the surface of PMo_{12}/ZrO_2.

TEM and HRTEM (figure 7a) images of the fresh catalyst indicate the non-crystalline and uniform dispersion of Pd(0) in the synthesized material. The dark uniform suspension in the amorphous nature of the catalyst (figure 7b) indicates the presence of very tiny Pd(0) nanoparticles (PdNPs) throughout the morphology without any aggregate formation, confirming the stabilization PdNPs by PMo_{12}.

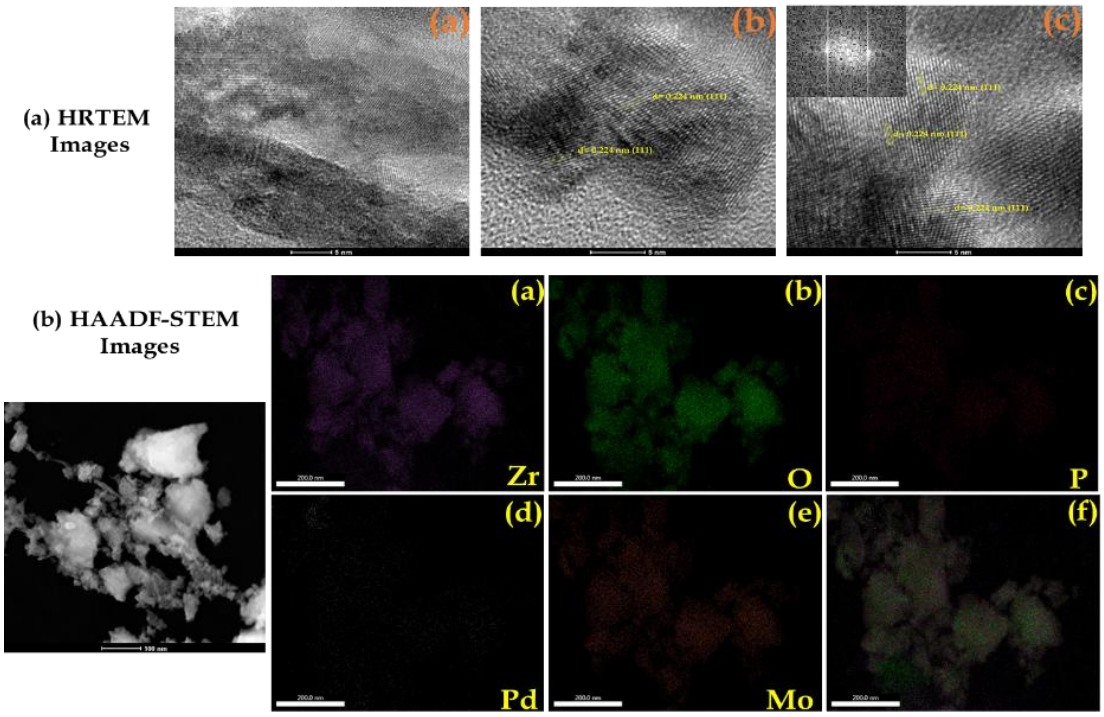

Figure 9. (a) HRTEM images and (b) HAADF-STEM images of fresh catalyst

The catalytic activity of the catalyst was evaluated towards One-pot Suzuki–Miyaura cross coupling/ nitro hydrogenation reaction. As we achieved excellent activity of Pd-PMA/ZrO_2 for SM cross-coupling, further Pd-PMo_{12}/ZrO_2 was evaluated for One-pot Suzuki–Miyaura cross coupling/ nitro

hydrogenation reaction. To achieve maximum conversion various reaction parameter were optimized such as, catalyst amount, pressure, time and temperature.

Based on above study, the optimized conditions for 100% conversion with 99% selectivity of 2-aminobiphenyl are: catalyst (50mg, active amount of Pd: 0.225 mg), 1-iodo-2-nitrobenzene (1.96 mmol), phenylboronic acid (2.94 mmol), K_2CO_3 (2.96 mmol), EtOH: H_2O (5:5 mL), pressure (10 bar), time (24 h) & temp. (90 °C) with, TON (918), TOF (38) and substrate ratio/ catalyst (927).

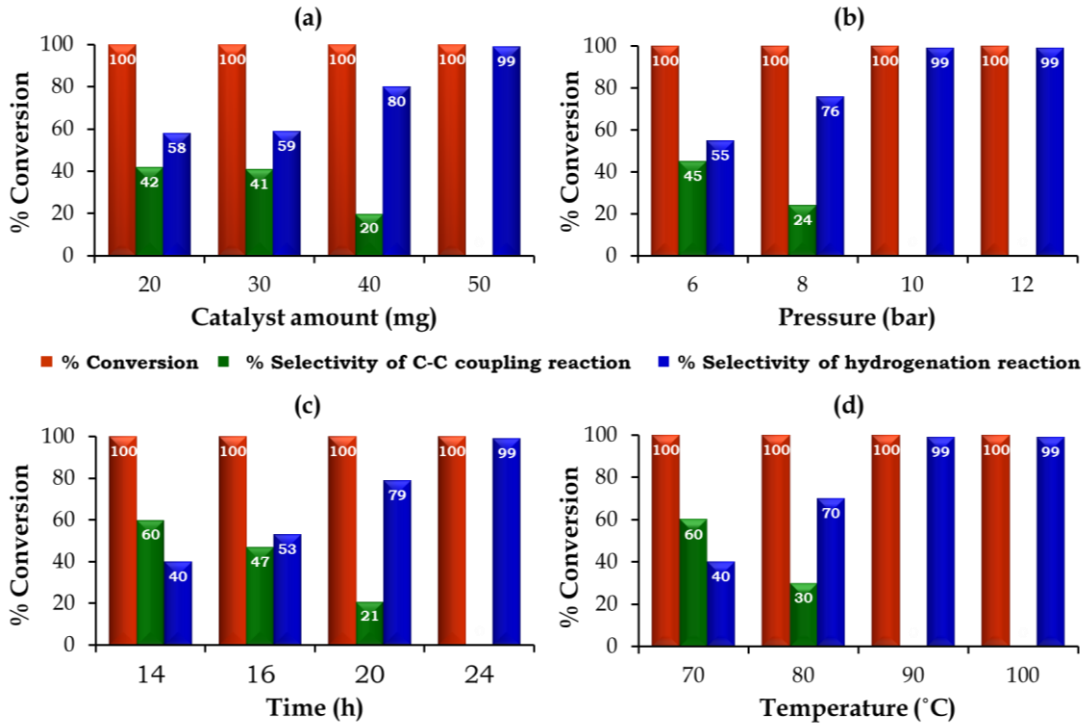

Figure 10. Optimization of reaction parameters for Tandem SM cross-coupling/ nitro hydrogenation reaction. Reaction condition: (a) Effect of catalyst amount- 1-iodo-2-nitrobenzene (1.96 mmol), phenylboronic acid (2.94 mmol), K_2CO_3 (3.92 mmol), EtOH: H_2O (5:5 mL), pressure (10 bar), time (24 h) and temp. (90 °C); (b) Effect of pressure- Catalyst (50 mg), 1-iodo-2-nitrobenzene (1.96 mmol), phenylboronic acid (2.94 mmol), K_2CO_3 (3.92 mmol), EtOH: H_2O (5:5 mL), time (24 h) and temperature (90 °C); (c) Effect of time- Catalyst (50 mg), 1-iodo-2-nitrobenzene (1.96 mmol), phenylboronic acid (2.94 mmol), K_2CO_3 (3.92 mmol), EtOH: H_2O (5:5 mL), pressure (10 bar) and temperature (90 °C); (d) effect of temperature. Catalyst (50 mg), 1-iodo-2-nitrobenzene (1.96 mmol), phenylboronic acid (2.94 mmol), K_2CO_3 (3.92 mmol), EtOH: H_2O (5:5 mL), pressure (10 bar) and time (24 h).

The control experiments were carried out with $PdCl_2$, PMo_{12}, ZrO_2, PMo_{12}/ZrO_2 and Pd-PMo_{12}/ZrO_2 under optimized conditions. It is seen from the obtained results that PMo_{12}, ZrO_2 and PMo_{12}/ZrO_2 are inactive towards the reaction. Almost same conversion was found in case of $PdCl_2$, and Pd-PMo_{12}/ZrO_2. This indicates that Pd is real active species responsible for the reaction.

The heterogeneity and recyclability tests were carried out for Pd-PMo_{12}/ZrO_2 by centrifuging the catalyst from the reaction mixture. This study also indicates that PMo_{12} plays an important role in binding the palladium very strongly and thus does not allow its leaching of palladium into the reaction mixture, making it, a true heterogeneous catalyst to recycle and reuse up to three cycles without any appreciable change in activity. In order to check the stability, the regenerated catalyst was characterized by EDX, FT-IR and XPS analysis which confirms the retention of catalyst structure and XRD indicates the presence of highly dispersed PdNPs over the surface of the catalyst, even after recycling.

Here, we propose the well-reported mechanism (scheme 7) for mechanistically two different catalytic transformations reactions. The SM C-C reaction involves oxidative addition, transmetallation and reductive elimination while in the case of nitro hydrogenation reaction we proposed universal hydride transfer via heterolytic cleavage of H_2.

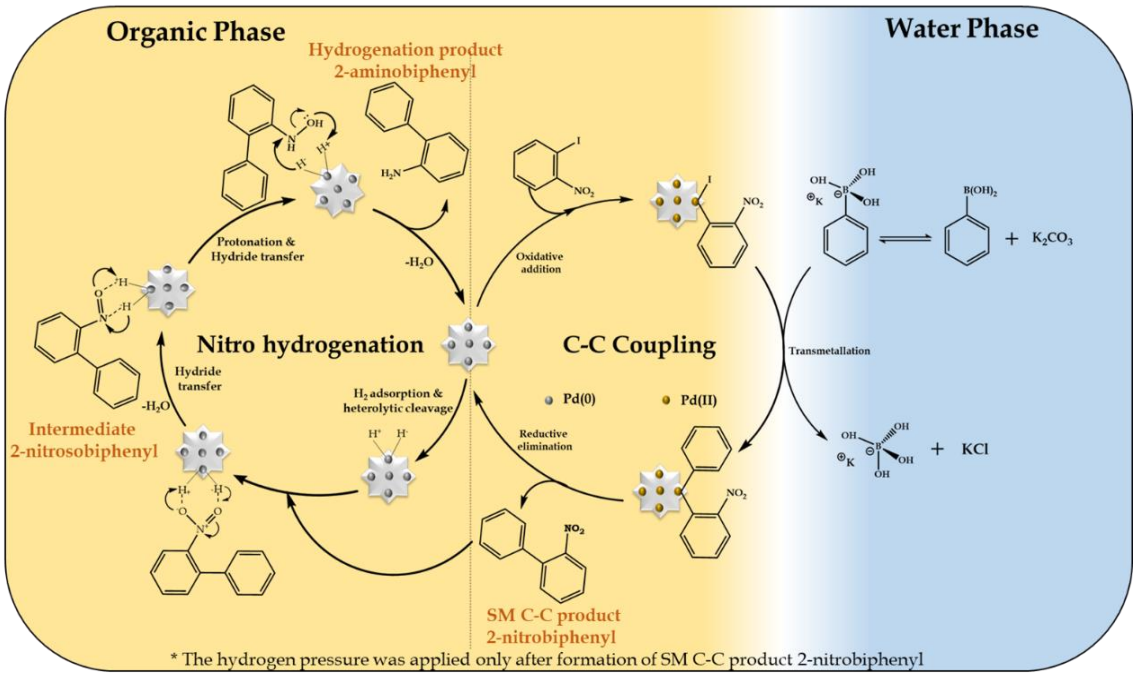

Scheme 7. Plausible Suzuki-Miyaura cross-coupling/ nitro hydrogenation reaction

Main Conclusion

- We have successfully designed catalytic materials comprising of transition metals (Fe, Ni and Pd) and phosphomolybdic acid by two different ways.
- The catalytic activity of all designed catalysts was evaluated towards hydrogenation (styrene, cyclohexene, levulinic acid and Tandem SM cross coupling/ nitro hydrogenation) reactions.
- For all reactions, the preference of the catalysts was found to be

  $PMo_{11}Fe$, $PMo_{11}Ni$ and $PMo_{11}Pd$ < **Fe-PMo_{12}/ZrO_2, Ni-PMo_{12}/ZrO_2 and Pd-PMo_{12}/ZrO_2**

  because of the structure diversity of suberates as well as position of metal.
- In all transformation, the TON number in the range of 927 – 5031 (>1000), indicating that all the catalysts can be applied for small scale industries.
- Our study confirmed that phosphomolybdic acid also acts as stabilization agent due to its unrivaled structural versality in both size and symmetry.

- Finally, the SASc designed strategy can be extended for the design of other precious metal-based single-atom site catalysts for various organic transformations.

Novelty of the Work

- Sustainable heterogeneous catalysts based on phosphomolybdic acid with excellent activity and TON were designed as an alternative to other environmentally hazardous catalysts for hydrogenation reactions
- For the first time, phosphomolybdic acid was utilized as a stabilizing agent for transition metals (Ni and Pd)
- The method for in-situ formation of Ni nanoparticles stabilized by phosphomolybdic acid was instituted for the first time
- Development of highly dispersed Pd Single Atom Site catalyst was accomplished and utilized for industrially important tandem Suzuki-Miyara cross-coupling/nitro hydrogenation reaction

Annexure: Nickel salt of phosphomolybdic acid (NiHPMA): Synthesis, characterization and application for oxidative esterification

NiHPMA was synthesized by direct method as reported in the literature with modification. 1 g of PMA was dissolved in minimum amount of distilled water followed by the addition of a stoichiometric amount of aqueous $Ni(CH_3CO_2)_2$ (58.6 mg) solution dropwise. The resulting mixture was aged for 1 h at 80 °C and the excess water was evaporated to dryness on water bath. The resulting material was oven dried at 100 °C for 10 h, calcined at 300 °C for 2 h and the obtained green coloured material was designated as NiHPMA.

Elemental analysis show the presence of all the expected elements and the found values for EDX values of the elements (P:1.39%, Mo:57.15%, Ni:2.89%, O:38.57%) were in good agreement with the that of the calculated values(P:1.54%, Mo:57.34%, Ni:2.92%, O:38.20%). TGA shows initial weight loss of 2.46 % up to 100 ^{0}C, due to the removal of adsorbed water. Further, it shows 4.11 % weight

loss up to 280 ^{0}C corresponding to removal of water of crystallization. After that, no appreciable weight loss was noticed, indicating the thermal stability of the synthesized material up to 500 ^{0}C. From the EDX and TGA, the chemical formula of the synthesized material was proposed as $NiH[PMo_{12}O_{40}].6H_2O$.

The UV-visible spectrum of NiHPMA (Figure 11a) shows the absorption peak at 230 nm due to the charge transfer between $O^{2-} \rightarrow Mo^{6+}$. Also it shows an absorption band at 396 nm, corresponding to the presence of Ni(II). FT-IR (Figure 11b) and Raman spectra of NiHPMA shows the presence of all the characteristic bands of PMA, which indicates the retention of the Keggin structure. The XPS spectra (Figure 11c) confirm the presence of Ni (II) and Mo (VI) oxidation states confirming no reduction of Mo(VI) during the synthesis of the materials.

The catalytic efficiency of the catalyst was evaluated for oxidative esterification of benzaldehyde. Based on above studies various reaction parameter, optimized conditions for maximum 68 % conversion with highest 86 % selectivity are: benzaldehyde, 10 mmol; H_2O_2, 30 mmol; catalyst, 5mg (active amount of Ni: 0.155 mg; catalyst/substrate ratio, 2.64×10^{-4}); methanol, 7 mL; temperature, 80 ^{0}C; and time, 6 hour, TON: 2576.

The control experiment indicates the bi-functional nature of catalyst where Mo contributes for oxidation and Ni for esterification due to its Lewis acidity. The catalyst is homogeneous even though it was easily recovered by simple heat to dryness method and used for number of cycles without significant change in conversion as well as selectivity. The characterization of regenerated catalyst confirmed that catalyst structure remains intact even after generation of catalyst. The substrate study shows that synthesised catalyst is highly viable towards variety of substrate.

To confirm either the reaction proceeds via formation of benzoic acid as intermediate, set of control experiments were carried out to confirm the same. The Mo and Ni contributes simultaneously in terms of Mo-peroxo spices for

oxidation while Ni-Oxo specie for esterification reaction was confirmed by UV-Visible and Raman spectroscopy respectively.

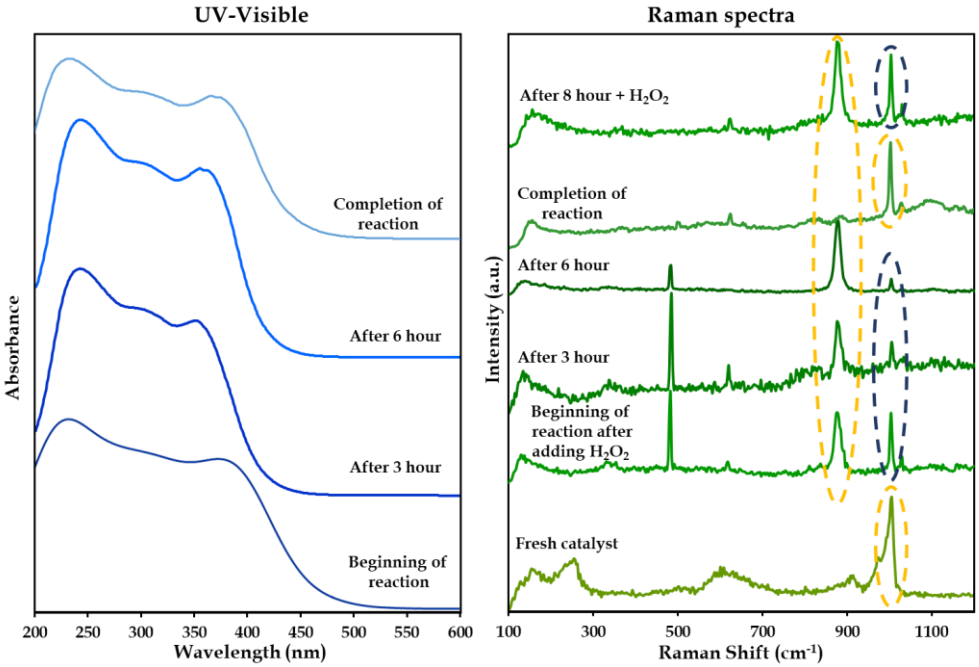

Figure 11. (a) UV-Visible and (b) Raman spectra at different time interval

Rferences

[1] J. C. Vedrine, Metal Oxides in Heterogeneous Catalysis, Elsevier, Saint Louis, (2018).

[2] M. L. Personick, M. M. Montemore, E. Kaxiras, R. J. Madix, J. Biener, C. M. Friend, Philos. trans., Math. phys. eng. sci., 374, 20150077, (2016).

[3] M. T. Pope, Y. Jeannin, M. Fournier, Heteropoly and isopoly oxometalates, Springer, (1983).

[4] C. L. Hill, C. M. Prosser-McCartha, Coord. Chem. Rev., 143, 407, (1995).

[5] T. Okuhara, N. Mizuno, M. Misono, Catalytic Chemistry of Heteropoly Compounds, in: D.D. Eley, W.O. Haag, B. Gates (Eds.) Advances in Catalysis, Academic Press, 113, (1996).

[6] R. Neumann, Polyoxometalate Complexes in Organic Oxidation Chemistry, Progress in Inorganic Chemistry, 317, (1997).

[7] N. Mizuno, M. Misono, Chem. Rev., 98, 199, (1998).

[8] I. V. Kozhevnikov, Chem. Rev., 98, 171, (1998).

[9] I. Kozhevnikov, Catalysis by polyoxometalates, John Wiley, Chichester, England Hoboken, NJ, (2002).

[10] N. Mizuno, K. Yamaguchi, K. Kamata, Coord. Chem. Rev., 249, 1944, (2005).

[11] N. Mizuno, S. Hikichi, K. Yamaguchi, S. Uchida, Y. Nakagawa, K. Uehara, K. Kamata, Catal. Today, 117, 32, (2006).

[12] L. Cronin, A. Müller, Chem. Soc. Rev., 41, 7333, (2012).

[13] D. Y. Du, J. S. Qin, S. L. Li, Z. M. Su, Y. Q. Lan, Chem. Soc. Rev., 43, 4615, (2014).

[14] Y. Ren, B. Yue, M. Gu, H. He, Materials, 3, 764, (2010).

[15] H. Lv, Y. V. Geletii, C. Zhao, J. W. Vickers, G. Zhu, Z. Luo, J. Song, T. Lian, D. G. Musaev, C. L. Hill, Chem. Soc. Rev., 41, 7572, (2012).

[16] M. Samaniyan, M. Mirzaei, R. Khajavian, H. Eshtiagh-Hosseini, C. Streb, ACS Catal., 9, 10174, (2019).

[17] C. T. Buru, O. K. Farha, ACS Appl. Mater. Interfaces, 12, 5345, (2020).

[18] Z. Wei, J. Wang, H. Yu, S. Han, Y. Wei, Molecules, 27, 1420, (2022).

[19] A. Dolbecq, E. Dumas, C. R. Mayer, P. Mialane, Chem. Rev., 110, 6009, (2010).

[20] Q. Li, L. Zhang, J. Dai, H. Tang, Q. Li, H. Xue, H. Pang, Chem. Eng. J., 351, 441, (2018).

[21] D. Wang, L. Liu, J. Jiang, L. Chen, J. Zhao, Nanoscale, 12, 5705, (2020).

[22] Y. Chen, F. Li, S. Li, L. Zhang, M. Sun, Inorg. Chem. Commun., 135, 109084, (2022).

[23] J. M. Clemente-Juan, E. Coronado, A. Gaita-Ariño, Chem. Soc. Rev., 41, 7464, (2012).

[24] O. Oms, A. Dolbecq, P. Mialane, Chem. Soc. Rev., 41, 7497, (2012).

[25] R. Sivakumar, J. Thomas, M. Yoon, J. Photochem. Photobiol. C: Photochem. Rev., 13, 277, (2012).

[26] N. I. Gumerova, A. Rompel, Inorg. Chem., 60, 6109, (2021).

[27] Y. Wang, I. A. Weinstock, Chem. Soc. Rev., 41, 7479, (2012).

[28] Q. Liu, X. Wang, Matter, 2, 816, (2020).

[29] J. M. Cameron, G. Guillemot, T. Galambos, S. S. Amin, E. Hampson, K. Mall Haidaraly, G. N. Newton, G. Izzet, Chem. Soc. Rev., 51, 293, (2022).

[30] P. Yin, D. Li, T. Liu, Chem. Soc. Rev., 41, 7368, (2012).

[31] M. Moors, J. Warneke, X. López, C. de Graaf, B. Abel, K. Y. Monakhov, Acc. Chem. Res., 54, 3377, (2021).